PROGRESS IN COLOR, COLORANTS AND COATINGS

available online @ www.pccc.icrc.ac.ir

Progress in Color Colorants Coating 16 (2023), 271-281

Ministry of Science, Research and Technology
Institute for Color Science & Technology

Facile One-pot Synthesis of Binder-free $MnCo_2O_4$ Nanosheets as Efficient Supercapacitor Electrode Material

Z. Norouzi, S. H. Mahmoudi Najafi, S. A. Mozaffari*

Department of Chemical Technologies, Iranian Research Organization for Science and Technology (IROST), P.O. Box: 33535-111, Tehran, Iran

ARTICLE INFO

Article history:
Received: 30 Oct. 2022
Final Revised: 23 Feb. 2023
Accepted: 28 Feb. 2023
Available online: 23 July 2023

Keywords:
Electrodeposition
$MnCo_2O_4$
Nanosheet arrays
Supercapacitor

ABSTRACT

The engineered nanostructured electrode material is an important factor in enhancing the performance of supercapacitors. Herein, a facile procedure was reported for the electrosynthesis of $MnCo_2O_4$ nanosheets through one-pot electrodeposition method. The obtained $MnCo_2O_4$ nanosheets have been characterized using field-emission scanning electron microscopy (FE-SEM), X-ray diffraction (XRD), and energy-dispersive X-ray spectroscopy (EDX) techniques. The results showed that $MnCo_2O_4$ nanosheets with multiple walls had been successfully prepared. The electrochemical evaluation revealed that the as-prepared $MnCo_2O_4$ electrode delivered a high specific capacitance of 1198 mF cm^{-2} at the current density of 1 mA cm^{-2} and demonstrated outstanding cycling performance. The binary nature of the $MnCo_2O_4$ nanosheets, along with the unique nanosheet architecture with accessible void spaces for the transfer of electrolyte ions and electrons, is responsible for these remarkable properties. These results demonstrate that the present $MnCo_2O_4$ nanosheets with outstanding electrochemical properties can be considered as promising candidates for energy storage systems. Prog. Color Colorants Coat. 16 (2023), 271-281© Institute for Color Science and Technology.

1. Introduction

Rapid reduction of fossil fuel supplies and the increase of greenhouse gases have caused a severe threat to the ecology of the earth. Also, with the increase of power demand for portable electronics, developing renewable and clean energy resources is necessary [1, 2]. In this regard, supercapacitors have attracted significant research interests from both industry and science due to their high power density, long cycle life, safe operation, and environmental friendliness [3] as backup/auxiliary power supplies of portable electronics, smart grids [4, 5], hybrid electric vehicles, and several micro-devices [6, 7].

Supercapacitors (i.e., electrochemical capacitors) can store charges on highly porous electrode materials. According to the charge storage mechanisms, they can be categorized into electrical double-layer capacitors (EDLCs) and pseudocapacitors [8]. The EDLC version is the most common type of supercapacitors and stores charges at the interface of electrode/electrolyte based on Helmholtz law. The pseudocapacitor version stores charges based on electrochemical reactions [9].

Many efforts have been made to develop high-performance electrode materials with low cost and high capacitance. The specific surface area of the electrode materials should be increased to increase the specific capacitance of supercapacitors. In this case, the EDLC capacitances promoted and imparted many electroactive

*Corresponding author: * mozaffari@irost.ir
Doi: 10.30509/pccc.2023.167053.1194

sites for participation in the electrochemical reaction. Furthermore, the suitable pore size distribution of the porous electrode materials facilitates the mass transfer of electrolyte ions through the pores for fast faradaic reactions and EDLC charging/discharging [10]. Hence, control over the dimensions and morphology of electrode material is vital for achieving high-performance supercapacitors [11].

Despite architecture, the material selection also plays an essential role in the performance of supercapacitors. Transition metal oxides (TMOs) and hydroxides, and conducting polymers as pseudocapacitor electrode materials offer higher electrochemical performances than carbonaceous materials (EDLC type) due to the contribution of redox reactions [12, 13]. Using binary transition metal oxides compared to single-component metal oxides is significant in enhancing electrochemical performance since they have different oxidation states and provide richer faradaic reactions, resulting in higher capacitances compared than single-metal oxides [14]. Among the most binary metal oxides, $MnCo_2O_4$ has been recognized as an attractive electrode material due to its higher electrochemical performance than unitary manganese oxide (MnO_2) and cobalt oxide (Co_3O_4) [15].

Till now, different Mn-Co oxide morphologies, such as $MnCo_2O_4$ nanorods [16], $MnCo_2O_4$ core-shell structures [17], and $MnCo_2O_4$ hollow nanotubes [18], have been reported for supercapacitor applications. Between different morphologies, 3D nanosheets directly grown on conductive substrates are considered an ideal architecture for supercapacitor application. They possess high electroactive sites and thin wall thickness, allowing easier electron transfer [19, 20]. A significant challenge in using $MnCo_2O_4$ as the electrode material in a supercapacitor is improving its electroactive sites by developing a facile one-pot route. Therefore, specific capacitance and cycling stability are enhanced [21]. Binders and additives used in the fabrication of electrodes usually block the electroactive sites of the electrode material and decrease the total efficacies [22]. Direct growth of nanosheets on conductive current collectors enhances the conductivity of the electrode materials by close contact of nanosheets to the current collector. Such a design does not require further additives or binders [19]. So, it is critically important to develop a facile approach for the synthesis of nanosheet electrode materials. Nickel foam substrates could be used as both current collector and structure support, and the electrode materials could be directly grown on them. In electrosynthesis, no binder and additive are used to prepare electrodes to prevent "dead" volume resulting from the tedious process of mixing active ingredients with polymer binder/conductive additives, and the total mass of the final device could be reduced.

A possible approach for decreasing the mass loading issues is precisely designing the $MnCo_2O_4$-based nano-architectures with a facile and cost-effective electrodeposition method to fulfill the requirement of high-rate supercapacitors [23]. Electrodeposition is a versatile method for fabricating porous electrode materials, which could produce many nano-architectures by tuning the processing factors [24].

To the best of our knowledge, the direct growth of $MnCo_2O_4$ nanosheets on Ni foam current collector has rarely been reported. Herein, we designed a facile, one-pot route for electro-synthesizing of 3D $MnCo_2O_4$ nanosheet arrays on the conductive substrate as an efficient binder-free electrode with enhanced surface area and easy ion and electron diffusion path. This method provides a higher utilization rate of the electrode material for high-rate supercapacitors. The resultant electrode revealed ultrahigh specific capacitance (1198 mF cm^{-2} at 1 mA cm^{-2}) and excellent cycle life (97 % capacitance retention after 2000 cycles at the scan rate of 250 mV s^{-1}), which is desired for energy storage applications.

2. Experimental

2.1. Synthesis of 3D $MnCo_2O_4$ nanosheets

All the reagents and chemicals were of analytical grade and were used without further purification. $MnCo_2O_4$ was synthesized through electrochemical deposition from the solution containing 5 mM $MnCl_2.6H_2O$, 5 mM $CoCl_2.6H_2O$, and 0.1 M KCl. Before electrodeposition, Ni foam was washed ultrasonically with alcohol, acetone, and deionized water for 10 min, respectively. All experiments were performed in a three-electrode configuration using cleaned Ni foam as the working electrode, Pt wire and Ag/AgCl as the auxiliary and reference electrodes, respectively. A potential of -1.0 V was applied against the Ag/AgCl for the duration of 120 and 1200 s. Then the samples were washed with distilled water several times and annealed at 200 °C for 30 min with temperature programming of 5 °C min^{-1}.

2.2. Characterization

The morphology and textural parameters of the nanosheets were monitored using field-emission scanning electron microscopy (FE-SEM, MiraII from TESCAN Company) equipped with energy-dispersive X-ray spectroscopy (EDX). The crystalline structure and purity of the prepared electrode were monitored by X-ray diffraction (XRD) using Philips PW 1730 diffractometer equipped with a Cu-K_α (λ=0.15418 nm) radiation source. Data were collected by scanning in the range of 10 ° to 80 ° with a step size of 0.05 ° (2θ) under grazing incidence mood.

2.3. Electrochemical measurement

The electrochemical tests were carried out at room temperature. The conventional three-electrode cell was used, which is connected to an Autolab PGSTAT.302N potentiostat/galvanostat (Eco-Chemie, The Netherlands). The deposited $MnCo_2O_4$ nanosheets on Ni foam substrate, Ag/AgCl electrode, and Pt plate were used as the working, reference, and auxiliary electrodes, respectively, in a solution of 3 M KOH as the electrolyte.

3. Results and Discussion

3.1. Synthesis and surface morphology analysis

A facile one-pot approach was used to deposit 3D $MnCo_2O_4$ nanosheets on Ni foam substrate (Figure 1) as an effective binder-free electrode. The electrodeposition bath contained a solution of $MnCl_2.6H_2O$, $CoCl_2.6H_2O$, and KCl. It took only 1200 s to deposit nanostructures with high specific capacitance completely. In practice, the weight of the cell is important, which could be affected by the electrolyte, binder, separator, collectors, and packaging material. The binder sticks the electrode materials on the substrate in both batteries and supercapacitors. However, the conductive additive is used to improve the electrical conductivity of the laminate. Using insulating polymeric binders increases the contact resistance between electroactive materials, which results in increased equivalent series resistance (ESR) value in the final device [25]. The binders and additives together constitute 20–40 % of the total mass of the electrode, namely 'dead mass', since it does not participate in charge storage, but instead lowers the specific energy of the final device. Besides, the diffusion path of ions and electrons is ambiguous due to the heterogeneous nature of the mixture, which results in low specific power and slow rate performance. The binder-less electrodes provide some advantages, comprising low weight, diverse macroscopic structures, well-defined pore size and distribution, and mechanical stability. It also offers higher output voltage and fast energy storage [26, 27]. Besides, such a design eliminates the need for expensive binders and additives, which reduces the cost and avoids the difficulty in electrode preparation processes.

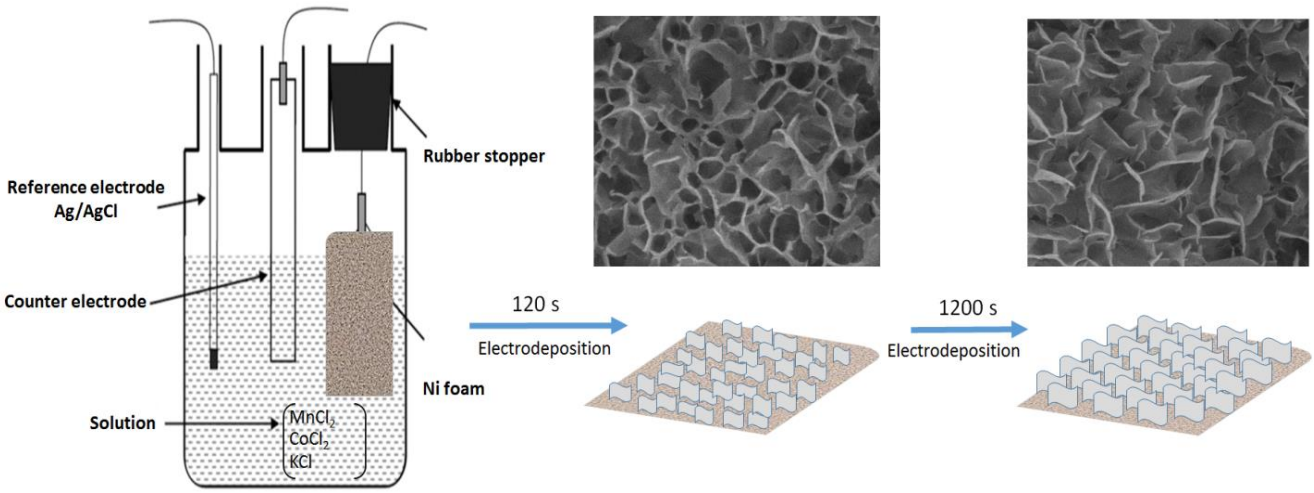

Figure 1: Schematic illustration of $MnCo_2O_4$ nanosheets synthesis.

FE-SEM is used to study the morphological features of the prepared electrodes. Figures 2a and b displays the FE-SEM images of the $MnCo_2O_4$ nanosheets on Ni foam substrate after 120 s. As shown, the nanosheet morphology was growing. The well-defined nanosheet morphology could be fully imaged by increasing the reaction time to 1200 s (Figures 2c and d. The $MnCo_2O_4$ nanosheets were vertically aligned and intertwined and formed 3D nanosheet arrays, which grew densely on the Ni foam substrate. After annealing at 200 °C, the $MnCo_2O_4$ keeps the wall-like architecture of the original morphology and becomes narrower. Figures 2e and f displays the SEM images of the $MnCo_2O_4$ nanosheets after annealing. The water has evaporated, and many open pores can be detected on the $MnCo_2O_4$ nanosheet surface. The 3D nanosheet structures obtained by electrodeposition clarify a high superficial area with an open mesoporous structure.

The nanosheets have an average diameter and length of about 15-30 nm and 1 μm, respectively (Figure 2F). With such a fascinating structure, the voids between the 3D $MnCo_2O_4$ nanosheet arrays can be efficiently utilized. Such a design shortens ion diffusion pathways [28]. It provides a fast ion and charges transportation path during the faradaic reactions and many electroactive sites for trapping and accumulating electrolyte ions [29].

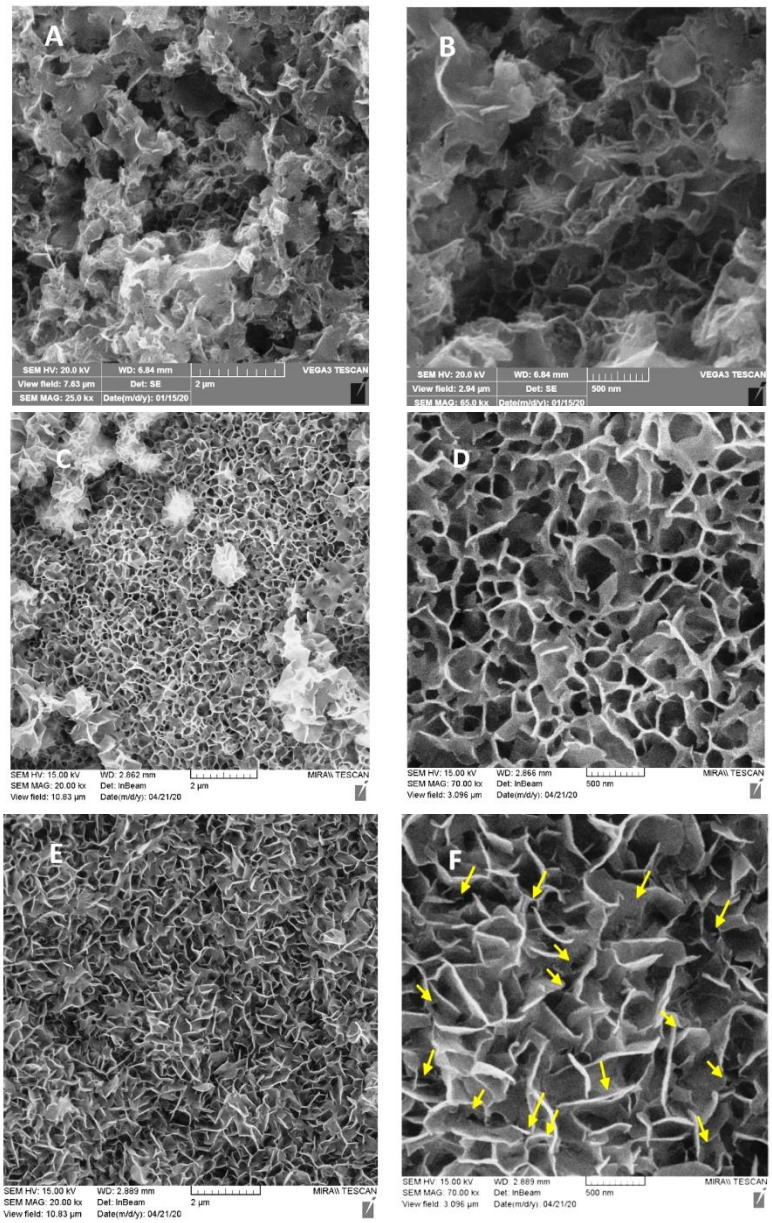

Figure 2: SEM images of $MnCo_2O_4$ nanosheets (A, B) after 120 s, (C, D) after 1200 s without annealing, (E, F) after 1200 s with annealing. Yellow arrows indicate some mesopores.

3.2. Crystalline structure

The elemental composition and crystalline structure of the prepared electrode were monitored by EDX and XRD analyses. The EDX spectrum in Figure 3a displays the presence of Mn, Co, and O elements. It can be seen in the XRD pattern (Figure 3b) that the intensity of three peaks at 44.5, 51.8, and 76.4 is much higher than the other peaks, which correspond to (1 1 1), (2 0 0), and (2 2 0) crystal facet of nickel in Nickel foam (JCPDS card no. 04-0850). The weak diffraction peaks appeared at 63.3° and 66.8°, which is consistent with (4 4 0), (5 3 1) crystal faces of spinel $MnCo_2O_4$ (JCPDS card no. 23–1237) as has been reported in the other references [30-33]. In most of the research reports, the XRD patterns of $MnCo_2O_4$ nanoscale compounds on nickel foam were very noisy, and the reflection peaks had low intensities. Also, maybe some reflection peaks of Co were hidden under Ni reflection peaks.

The sample with the less intense diffraction peak shows that the scale of the nanostructure is small, which can increase the number of effective electrochemical reaction points to improve the electro-chemical performance [34].

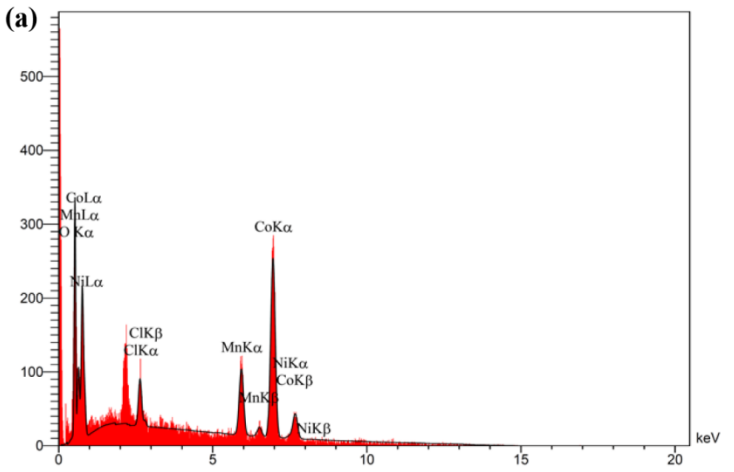

Quantitative Results

Elt	Line	Int	Error	K	Kr	W%	A%	ZAF	Formula	Ox%	Cat#
O	Ka	69.5	15.0636	0.1264	0.1134	18.04	43.90	0.6285		0.00	0.00
Cl	Ka	31.9	1.2193	0.0302	0.0271	3.04	3.34	0.8923		0.00	0.00
Mn	Ka	61.2	0.6953	0.1597	0.1432	13.05	9.25	1.0976		0.00	0.00
Co	Ka	171.8	0.6953	0.6712	0.6021	64.71	42.74	0.9305		0.00	0.00
Ni	Ka	2.5	0.6953	0.0125	0.0113	1.17	0.77	0.9648		0.00	0.00
				1.0000	0.8970	100.00	100.00			0.00	0.00

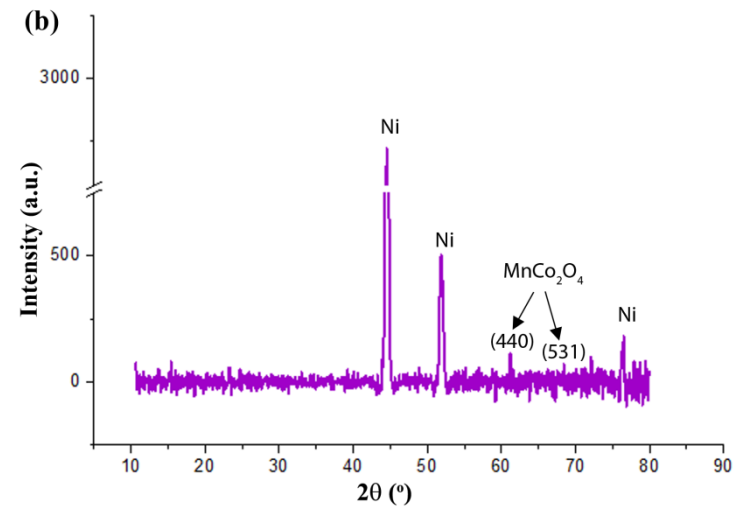

Figure 3: (a) EDX spectrum and (b) XRD pattern of $MnCo_2O_4$ nanosheets on the Ni foam.

3.3. Electrochemical evaluation

The super capacitive performance of the electro-synthesized electrode was investigated in this paper. Cyclic voltammetry (CV), galvanostatic charge/discharge (GCD), and electrochemical impedance spectroscopy (EIS) were used. They were measured in a three-electrode setup in 3 M KOH solution as the electrolyte.

3.3.1. Cyclic voltammetry

The CV curve was first recorded at 10 mV s^{-1} within the potential range of 0.0 to 0.5 V, as shown in Figure 4(a). The shape of the CV curve is different from that of EDLCs, which is similar to an ideal rectangular shape. The CV curves of the $MnCo_2O_4$ electrode show a pair of redox peaks corresponding to the interaction between spinel materials and electrolyte ions, reflecting the pseudocapacitive nature of the electrodes [35]. For the $MnCo_2O_4$ nanosheets, the electrochemical reactions could be described according to the following equation (Eq.1) [36]:

$$MnCo_2O_4 + OH^- + H_2O \longleftrightarrow MnOOH + 2CoOOH + e^- \quad (1)$$

Based on the CV curve (Figure 4) of the $MnCo_2O_4$ electrode, a reversible electron-transfer process was detected, suggesting that the capacitance of $MnCo_2O_4$ arises from the redox mechanism. Furthermore, the low surface area obtained from the Ni foam substrate proves that the capacitance due to the current collector is negligible, and does not contribute to electrochemical reactions.

Figure 4b shows the CV curves of the $MnCo_2O_4$ electrode at different scan rates (5-100 mV s^{-1}). By increasing the scan rate, CV curves retain a nearly constant shape, representing the outstanding rate capability and fast kinetic of the faradaic reactions [37]. A slight shift in the anodic peaks was ascribed to the internal resistance of the electrode. At lower scan rates, the electrolyte ions can intercalate/de-intercalate into the accessible sites in the $MnCo_2O_4$ nanosheets, which results in high electrochemical reactions and high capacitance. But at higher scan rates, the effective interaction between electrode/electrolyte is considerably decreased. The faradaic reactions can take place only on the electrode material's outer surface, which leads to a decrease in the total capacitance [38].

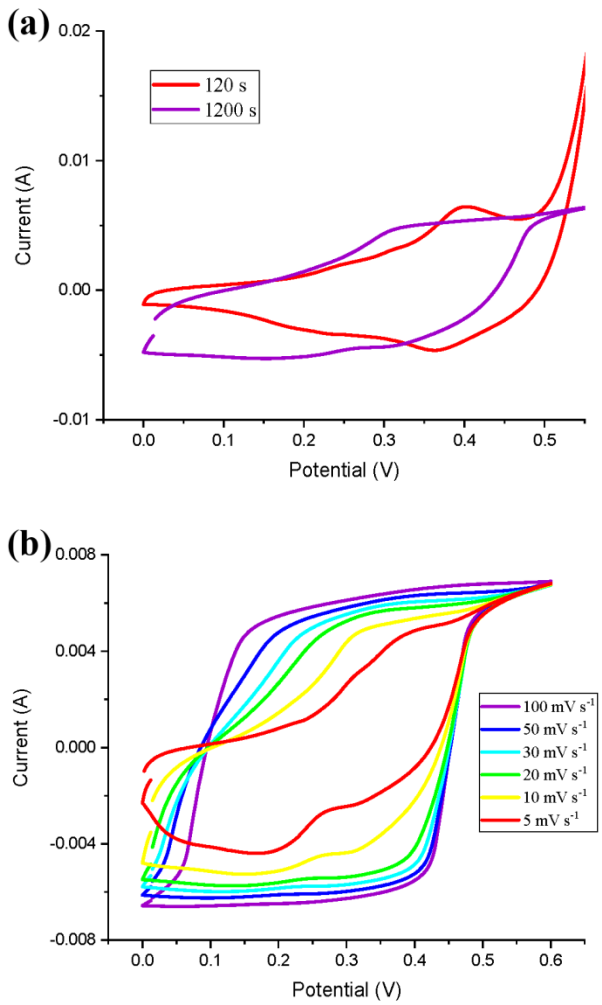

Figure 4: Voltammograms of $MnCo_2O_4$ nanosheets (a) at different deposition times at 10 mV s^{-1}, (b) at deposition time of 1200 s at different scan rates.

3.3.2. Galvanostatic charge/discharge

Figure 5a provides the GCD curve of the $MnCo_2O_4$ electrode with different deposition times in a potential window of 0.0-0.45 V (*vs.* Ag/AgCl) at the current density of 1.0 mA cm^{-2}. The symmetric shape of the GCD curves with the two well-defined voltage plateaus suggests the pseudocapacitive behavior of the electrode during the charge/discharge processes. It confirms the reversibility of the redox reactions [39], which agrees with CV results. The specific capacitance (mF cm^{-2}) was determined from the discharge cycles using equation 2 [40]:

$$C_s = \frac{I\Delta t}{S\Delta V} \quad (2)$$

where *I* is the charge/discharge current (A), Δ*t* is the discharge time (s), *S* is the surface area of electrode material (cm^2), and Δ*V* is the potential range during discharge (V). According to the discharge time, increasing deposition time remarkably affected the specific capacitance. The $MnCo_2O_4$ electrode with a deposition time of 1200 s delivered a high specific capacitance of 1198 mF cm^{-2} at the current density of 1.0 mA cm^{-2}, while the $MnCo_2O_4$ electrode with the deposition time of 120 s delivered a specific capacitance of 577 mF cm^{-2} at the same current density.

Figure 5b shows the GCD curves of the $MnCo_2O_4$ nanosheet electrode at different current densities, ranging from 1 to 20 mA cm^{-2}. The curves are symmetric, and the duration of charge and discharge curves are nearly equal, indicating a high columbic efficiency, fast redox reactions at the interface of electrode/electrolyte, and ideal capacitor behavior.

3.3.3. Electrochemical impedance spectroscopy (EIS)

The EIS analysis is a significant test that provides valuable information about the resistance behavior at the interface of electrode/electrolyte in many applications [41-51]. The Nyquist impedance plot (imaginary part (Z'') versus real part (Z')) for the $MnCo_2O_4$ nanosheet electrode shows a small semicircle in a high-frequency region and a nearly straight line in the low-frequency region.

The intercept of the Nyquist plot at the x-axis reflects the equivalent series resistance (ESR) value. At the same time, the diameter of the semicircle represents the charge-transfer resistance (R_{ct}) value, and the straight line at the low-frequency region reflects the Warburg impedance. The ESR value of the $MnCo_2O_4$ nanosheet electrode achieved from extrapolating the Nyquist plot at the x-axis was 1.65 Ω (Figure 6a), which arose from the resistance of both electrolyte and electrode textile. The low ESR value of the electrode reveals fast electron transfer, reflecting the rich electrochemical reactions of the $MnCo_2O_4$ nanosheet.

According to the diameter of the semicircle (indicative of interfacial charge-transfer resistance), the R_{ct} of the $MnCo_2O_4$ nanosheet electrode was 2.5 Ω. The high electrical conductivity of $MnCo_2O_4$ resulted in the reduced R_{ct} and can be related to the fast charge transfer rate of the ions at $MnCo_2O_4$ nanosheets. Besides, the sharp line at the high-frequency region reflects the Warburg resistance (the more vertical line for an electrode closer to an ideal capacitor), which arises from the frequency dependence of ion diffusion in the electrolyte [52, 53]. The $MnCo_2O_4$ nanosheets revealed a short ion diffusion pathway, as shown from the Warburg part on the Nyquist plot.

Furthermore, the $MnCo_2O_4$ electrode displays an almost vertical line in the low-frequency region, indicating reduced mass transfer resistance (Warburg), and further approving the fast redox reactions. Moreover, the $MnCo_2O_4$ nanosheet shows a lower internal resistance indicating its higher electrical conductivity [16].

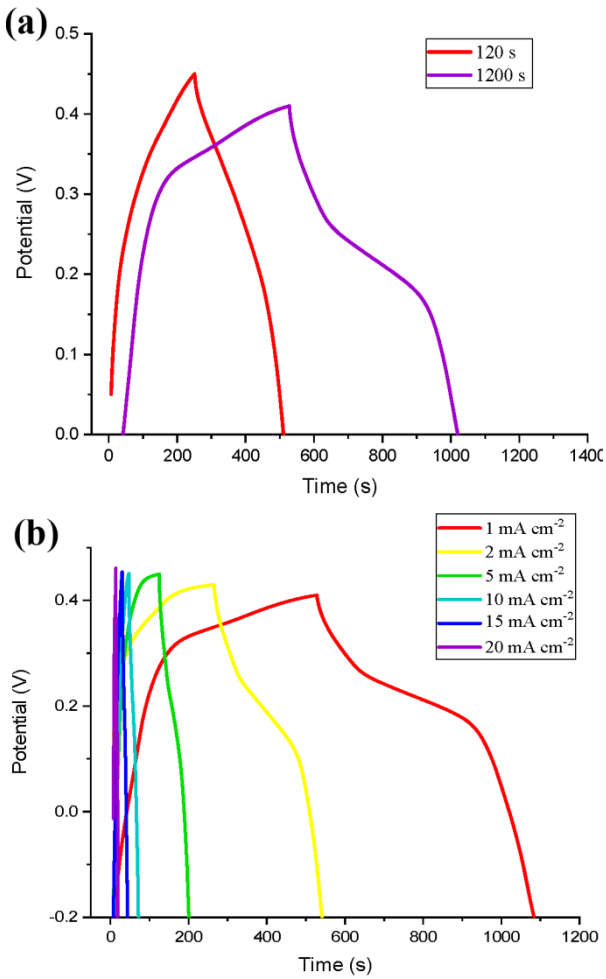

Figure 5: GCD curves of $MnCo_2O_4$ nanosheets (a) at different deposition times at 1 mA cm^{-2}, (b) at deposition time of 1200 s at different current densities.

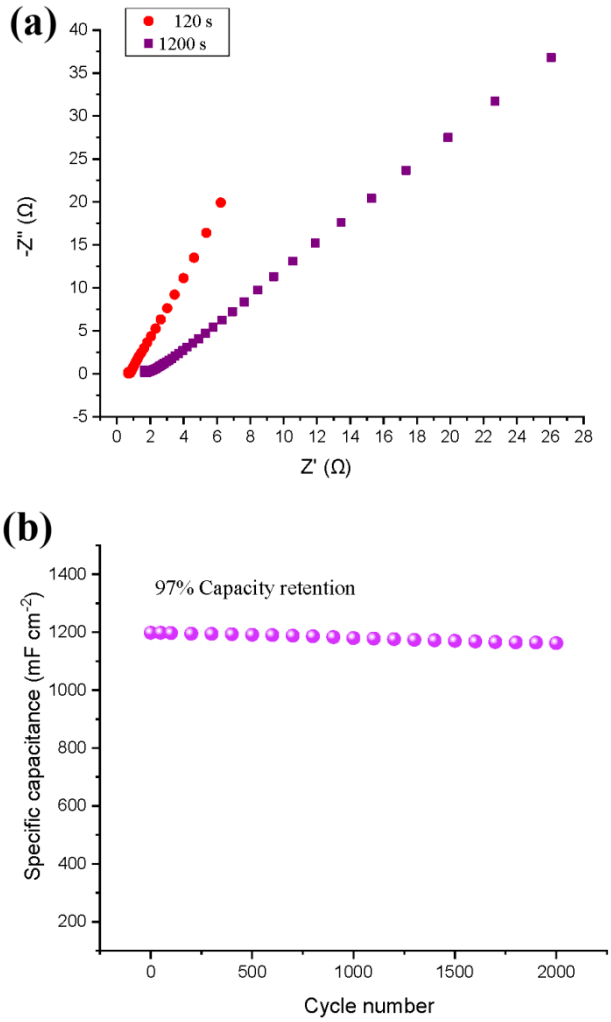

Figure 6: (A) EIS of $MnCo_2O_4$ nanosheets at different deposition times, and (B) capacity retention of $MnCo_2O_4$ nanosheets after 2000 CCV curve at 250 mV s^{-1}.

3.3.4. Continues cyclic voltammetry (CCV)

Long-term cycling stability is necessary for practical application of supercapacitors. It was examined for the $MnCo_2O_4$ nanosheet electrode. CCV test can be regarded as the best technique for monitoring and exploring the CVs and charge storage performance of supercapacitors during the time [54-56]. Successive CCV tests estimated the long-term cycling stability of the $MnCo_2O_4$ nanosheet electrode at the scan rate of 250 mV s^{-1} for 2000 cycles.

The specific capacitance as a function of time is demonstrated in Figure 6b. As shown, the specific capacitance of the $MnCo_2O_4$ nanosheet electrode remains nearly unchanged until 2000 cycles and gradually decreases from 1198 mF cm^{-2} to 1162 mF cm^{-2} (3% decrease). This phenomenon suggests the excellent cycling stability of the $MnCo_2O_4$ electrode. These results reveal that the $MnCo_2O_4$ nanosheet electrode is highly stable during the time. The enhanced electrochemical performance of the $MnCo_2O_4$ nanosheet arrays was ascribed to its unique structure, which provides more electroactive sites for reactive species.

The superior performance of the $MnCo_2O_4$ electrode can be ascribed to the following features: (1) The $MnCo_2O_4$ was directly grown on a nickel foam substrate, which can gain direct mechanical and electrical contact with the underlying nickel foam. (2) The nanosheet feature of the $MnCo_2O_4$ electrode and superior contact area provide many electroactive sites for ions adsorption and electrochemical redox reactions. (3) The voids between the interconnected nanosheets act as ion-buffering reservoirs and ease the channeling of electrolyte ions and charge transfer [57, 58]. (4) The spinel nature of the $MnCo_2O_4$ nanosheets has high electrical conductivity and rich redox reaction, providing many superficial electroactive species for participation in Faradaic redox reactions. Therefore, lower contact resistance and superior super capacitive performance can be obtained [59]. (5) Binder-free design provides efficient electron paths for charge transport because of void spaces between neighboring sheets and ensures efficient electron transfer between active material and substrate. All of these aspects are beneficial for enhancing the super capacitive performances of the electrode materials.

4. Conclusions

In summary, a facile one-pot approach has been developed to deposit 3D interconnected $MnCo_2O_4$ nanosheet arrays through electrochemical deposition on Ni foam substrate as an efficient electrode material for supercapacitors. The $MnCo_2O_4$-loaded nickel foam can be directly used as a supercapacitor electrode without any binders and/or additives. The $MnCo_2O_4$ nanosheet electrode revealed superior performances, including a high specific capacitance of 1198 mF cm^{-2} at 1 mA cm^{-2} and long cycle life. The improved super capacitive performances are mainly ascribed to its unique nanosheet architecture, which provides many electroactive sites for electrolyte ions, allowing them easy access to the electrode surface. The results are

promising and indicate the possible application of $MnCo_2O_4$ nanosheets as electrode material for supercapacitors.

Acknowledgment

S. A. Mozaffari acknowledges the support rendered by the Iranian Research Organization for Science and Technology (IROST), and Iran Nanotechnology Initiative Council (INIC).

5. References

1. S. Zhang, N. Pan, Supercapacitors performance evaluation, *Adv. Energy Mater*., 5(2015), 1401401.
2. L. Huang, D. Chen, Y. Ding, S. Feng, Wang Z.L., M. Liu, Nickel–cobalt hydroxide nanosheets coated on $NiCo_2O_4$ nanowires grown on carbon fiber paper for high-performance pseudocapacitors, *Nano Lett.*, 13(2013), 3135-3139.
3. P. Simon, Y. Gogotsi, B. Dunn, Where do batteries end and supercapacitors begin?, *Science*, 343(2014), 1210-1211.
4. X. Cao, B. Zheng, W. Shi, J. Yang, Z. Fan, Z. Luo, X. Rui, B. Chen, Q. Yan, H. Zhang, Reduced graphene oxide-wrapped MoO_3 composites prepared by using metal–organic frameworks as precursor for all-solid-state flexible supercapacitors, *Adv. Mater*., 27(2015), 4695-4701.
5. L. F. Chen, Z. H. Huang, H. W. Liang, Q. F. Guan, S. H. Yu, Bacterial-cellulose-derived carbon nanofiber@ MnO_2 and nitrogen-doped carbon nanofiber electrode materials: An asymmetric supercapacitor with high energy and power density, *Adv. Mater*., 25(2013), 4746-4752.
6. P. Simon, Y. Gogotsi, Materials for electrochemical capacitors. In Nanoscience and technology: a collection of reviews from Nature journals 2010 (pp. 320-329).
7. G. Wang, L. Zhang, J. Zhang, A review of electrode materials for electrochemical supercapacitors, *Chem. Soc. Rev*., 41(2012), 797-828.
8. L. Abbasi, M. Arvand, Engineering hierarchical ultrathin $CuCo_2O_4$ nanosheets array on Ni foam by rapid electrodeposition method toward high-performance binder-free supercapacitors, *Appl. Surf. Sci*., 445(2018), 272-280.
9. Z. Yu, L. Tetard, L. Zhai, J. Thomas, Supercapacitor electrode materials: nanostructures from 0 to 3 dimensions, *Energy Environ. Sci*., 8(2015), 702-730.
10. H. Zhou, D. Li, M. Hibino, I. Honma, A self-ordered, crystalline-glass, mesoporous nanocomposite for use as a lithium-based storage device with both high power and high energy densities, *Angew. Chem. Int. Ed*., 44(2005), 797-802.
11. D.N. Futaba, K. Hata, T. Yamada, T. Hiraoka, Y. Hayamizu, Kakudate Y. Kakudate, O. Tanaike, H. Hatori, M. Yumura, S. Iijima, Shape-engineerable and highly densely packed single-walled carbon nanotubes and their application as super-capacitor electrodes, *Nat. Mater*., 5(2006), 987-994.
12. H. Heydari, S.E. Moosavifard, S. Elyasi, M. Shahraki, Nanoporous CuS nano-hollow spheres as advanced material for high-performance supercapacitors, *Appl. Surf. Sci*., 394(2017), 425-430.
13. Z. Norouzi, S. A. Mozaffari, S. H. Mahmoudi Najafi, Three-dimensional unified electrode design using CuO embedded MnO_2 Nano-dandelions@$Ni(OH)_2$ nano-flakes as electrode material for high-performance supercapacitors, *J. Alloy. Compd.*, 938(2023), 168603.
14. L. Shen, L. Yu, H.B. Wu, X.Y. Yu, X. Zhang, X.W. Lou, Formation of nickel cobalt sulfide ball-in-ball hollow spheres with enhanced electrochemical pseudocapacitive properties, *Nat. Commun.*, 6(2015), 1-8.
15. L. Li, Y.Q. Zhang, X.Y. Liu, S.J. Shi, X.Y. Zhao, H. Zhang, X. Ge, G.F. Cai, C.D. Gu, X.L. Wang, J.P. Tu, One-dimension $MnCo_2O_4$ nanowire arrays for electrochemical energy storage, *Electrochim. Acta*, 116(2014) 467-474.
16. S. Jayasubramaniyan, S. Balasundari, P.A. Rayjada, R.A. Kumar, N. Satyanarayana, P. Muralidharan, Enhanced electrochemical performance of $MnCo_2O_4$ nanorods synthesized via microwave hydrothermal method for supercapacitor applications, *J. Mater. Sci. Mater. Electron*., 29(2018) 21194-21204.
17. J.A. Mehrez, K.A. Owusu, Q. Chen, L. Li, K. Hamwi, W. Luo, L. Mai, Hierarchical $MnCo_2O_4$@$NiMoO_4$ as free-standing core-shell nanowire arrays with synergistic effect for enhanced supercapacitor performance, *Inorg. Chem. Front*., 6(2019) 857-865.
18. L. Wu, J. Lang, P. Zhang, X. Zhang, R. Guo, X. Yan, Mesoporous Ni-doped $MnCo_2O_4$ hollow nanotubes as an anode material for sodium ion batteries with ultralong life and pseudocapacitive mechanism, *J. Mater. Chem. A*, 4(2016), 18392-18400.
19. G. Zhang, X.W. Lou, General solution growth of mesoporous $NiCo_2O_4$ nanosheets on various conductive substrates as high-performance electrodes for supercapacitors, *Adv. Mater*., 25(2013), 976-979.
20. D. Cai, S. Xiao, D. Wang, B. Liu, L. Wang, Y. Liu, H. Li, Y. Wang, Q. Li, T. Wang, Morphology controlled synthesis of $NiCo_2O_4$ nanosheet array nanostructures on nickel foam and their application for

pseudocapacitors, *Electrochim. Acta*, 142(2014), 118-124.
21. A.K. Mondal, D. Su, S. Chen, A. Ung, H.S. Kim, G. Wang, Mesoporous $MnCo_2O_4$ with a flake-like structure as advanced electrode materials for lithium-ion batteries and supercapacitors, *Chem. A Eur. J*., 21(2015), 1526-1532.
22. M. F. El-kady, Y. Shao, R. B. Kaner, Graphene for batteries, supercapacitors and beyond, *Nat. Rev. Mater.*, 1(2016), 1-14.
23. X. Xia, J. Tu, Y. Zhang, X. Wang, C. Gu, X. B. Zhao, H. J. Fan, High-quality metal oxide core/Shell nanowire arrays on conductive substrates for electrochemical energy storage, *acs nano*, 6(2012), 5531-5538.
24. R. P. Silva, S. Eugénio, T. M. Silva, M. J. Carmezim, Montemor M.F. Montemor, Fabrication of three-dimensional dendritic Ni-Co films by electrodeposition on stainless steel substrates, *J. Phys. Chem. C*, 116(2012), 22425-22431.
25. S-L. Chou, Y. Pan, J-Z. Wang, H-K. Liu, S-X. Dou, Small things make a big difference: binder effects on the performance of Li and Na batteries, *Phys. Chem. Chem. Phys*., 16(2014), 20347-20359.
26. D. Liu, Q. Wang, L. Qiao, F. Li, D. Wang, Z. Yang, D. He, Preparation of nano-networks of MnO_2 shell/Ni current collector core for high-performance supercapacitor electrodes, *J. Mater. Chem*., 22(2012), 483-487.
27. T. Fujita, P. Guan, K. McKenna, X. Lang, A. Hirata, L. Zhang, T. Tokunaga, S. Arai, Y. Yamamoto, N. Tanaka, Y. Ishikawa, Atomic origins of the high catalytic activity of nanoporous gold, *Nat. Mater*., 11(2012), 775-780.
28. Y. Zhang, M. Ma, J. Yang, C. Sun, H. Su, W. Huang, X. Dong, Shape-controlled synthesis of $NiCo_2S_4$ and their charge storage characteristics in supercapacitors, *Nanoscale*, 6(2014), 9824-9830.
29. S. Sahoo, C.S. Rout, Facile electrochemical synthesis of porous manganese-cobalt-sulfide based ternary transition metal sulfide nanosheets architectures for high performance energy storage applications, *Electrochim. Acta*, 220(2016), 57-66.
30. H. Liu, Z. Guo, S. Wang, X. Xun, D. Chen, J. Lian, Reduced core-shell structured $MnCo_2O_4$@MnO_2 nanosheet arrays with oxygen vacancies grown on Ni foam for enhanced-performance supercapacitors" *J. Alloy. Compd.*, 846(2020), 156504.
31. M. He, L. Cao, W. Li, X. Chang, X. Zheng, Z. Ren, NiO nanoflakes decorated needle-like $MnCo_2O_4$ hierarchical structure on nickle foam as an additive-free and high-performance supercapacitor electrode, *J. Mater. Sci.*, 56(2021), 8613-8626.
32. J. Xu, Y. Sun, M. Lu, L. Wang, J. Zhang, E. Tao, J. Qian, X. Liu, Fabrication of the porous $MnCo_2O_4$ nanorod arrays on Ni foam as an advanced electrode for asymmetric supercapacitors", *Acta Mater.*, 152(2018), 162-174.
33. S. Tan, Y. Ji, F. Chen, and W. Ouyang, Three-dimensional sea urchin-like $MnCo_2O_4$ nanoarchitectures on Ni foam towards high-performance asymmetric supercapacitors, *Front. Mater. Sci.*, 15(2021), 611-620.
34. Z. Chaozheng, M. Yongzhi, B. Qingkai, Z. Yanting, W. Kai, Two-step synthesis and characterization of $mnco_2o_4$ composite and its electrochemical performance, *Int. J. Electrochem. Sci.*, 13(2018), 10207-10216.
35. C. Yuan, L. Yang, L. Hou, L. Shen, X. Zhang, X.W. Lou, Growth of ultrathin mesoporous Co_3O_4 nanosheet arrays on Ni foam for high-performance electrochemical capacitors, *Energ. Environ. Sci.*, 5(2012), 7883-7887.
36. A. Pramanik, S. Maiti, M. Sreemany, S. Mahanty, Carbon doped $MnCo_2S_4$ microcubes grown on ni foam as high energy density faradaic electrode, *Electrochim. Acta*, 213(2016) 672-679.
37. S.E. Moosavifard, S. Fani, M. Rahmanian, Hierarchical $CuCo_2S_4$ hollow nanoneedle arrays as novel binder-free electrodes for high-performance asymmetric supercapacitors, *Chem. Commun*., 4(2016), 2-5.
38. A.A. Ensafi, S.E. Moosavifard, B. Rezaei, S.K. Kaverlavani, Engineering onion-like nanoporous $CuCo_2O_4$ hollow spheres derived from bimetal-organic frameworks for high-performance asymmetric supercapacitors, *J. Mater. Chem. A*., 6(2018), 10497-10506.
39. H. Jiang, T. Zhao, C. Li, J. Ma, Hierarchical self-assembly of ultrathin nickel hydroxide nanoflakes for high-performance supercapacitors, *J. Mater. Chem*., 21(2011), 3818-3823.
40. M. Amiri, S.E. Moosavifard, S.SH. Davarani, S.K. Kaverlavani, M. Shamsipur, MnCoP hollow nanocubes as novel electrode material for asymmetric supercapacitors, *Chem. Eng. J*., 420(2021), 129910.
41. M. Khalili, M. Abedi, H.S. Amoli, S.A. Mozaffari, Comparison of chitosan and chitosan nanoparticles on the performance and charge recombination of water-based gel electrolyte in dye sensitized solar cells, *Carbohyd. Polym*., 175(2017), 1-6.
42. E. Kouhestanian, S.A. Mozaffari, M. Ranjbar, H.S. Amoli, Enhancing the electron transfer process of TiO_2-based DSSC using DC magnetron sputtered ZnO as an efficient alternative for blocking layer, *Org. Electron*., 86(2020), 105915.
43. M. Seifpanah Sowmehesaraee, M. Ranjbar, M. Abedi, S.A. Mozaffari, Fabrication of lead iodide perovskite solar cells by incorporating zirconium, indium and zinc metal-organic frameworks, *Sol. Energy*, 214(2021), 138-148.
44. M. Emadoddin, S.A. Mozaffari, F. Ebrahimi, An antifouling impedimetric sensor based on zinc oxide embedded polyvinyl alcohol nanoplatelets for wide range dopamine determination in the presence of high concentration ascorbic acid, *J. Pharm. Biomed. Anal.*, 205(2021), 114278.

45. M. Hosseinzadeh, S. A. Mozaffari, F. Ebrahimi, Porous 3D-graphene functionalized with MnO_2 nanospheres and NiO nanoparticles as highly efficient electrodes for asymmetric capacitive deionization: Evaluation by impedance-derived capacitance spectroscopy, *Electrochim. Acta*, 427(2022) 140844.
46. S. Khazaei, S.A. Mozaffari, F. Ebrahimi, Polyvinyl alcohol as a crucial omissible polymer to fabricate an impedimetric glucose biosensor based on hierarchical 3D-NPZnO/chitosan, *Carbohyd. Polym.* 266 (2021), 118105.
47. R. Shabani, S.A. Mozaffari, S.W. Husain, M.S. Tehrani, Selective nanosensing of copper (II) ion using l-lysine functionalized gold cysteamine self-assembled monolayer, *Iran. J. Sci. Technol. Trans A Sci*., 33(2009), 335-347.
48. S.A. Mozaffari, S.H. Mahmoudi Najafi, Z. Norouzi, Hierarchical NiO@$Ni(OH)_2$ nanoarrays as high-performance supercapacitor electrode material, *Electrochim. Acta*, 368(2021) 137633.
49. A. Shahriari, H. Aghajani, M.Gh. Hosseini, A study of oxidation behavior of AZ91D alloy with YSZ coating using *EIS, Prog. Color Colorants Coat*., 10(2017), 1-12.
50. M.Gh. Hosseini, K. Aboutalebi, Electrochemical evaluation of corrosion protection performance of epoxy/polyaniline-imidazole modified ZnO nanocomposite coating on mild steel, *Prog. Color Colorants Coat.*, 10(2017), 181-192.
51. E. Kouhestanian, M. Ranjbar, S.A. Mozaffari, H. Salaramoli, Investigating the effects of thickness on the performance of ZnO-Based DSSC, *Prog. Color Colorants Coat.*, 14(2021), 101-112.
52. S.A. Hashemi, S.M. Mousavi, H.R. Naderi, S. Bahrani, M. Arjmand, A. Hagfeldt, W.H. Chiang, S. Ramakrishna, Reinforced polypyrrole with 2D graphene flakes decorated with interconnected nickel-tungsten metal oxide complex toward superiorly stable supercapacitor, *Chem. Eng. J*., 418(2021), 129396.
53. Z. Norouzi, S. H. Mahmoudi Najafi, S. A. Mozaffari, Silver-loaded carbon sphere-in-rod 3D nano-architectures as electrode material for supercapacitors, *Diam. Relat. Mater.*, 27(2021), 108734.
54. H.R. Naderi, A. Sobhani-nasab, M. Rahimi-nasrabadi, M.R. Ganjali, Decoration of Nitrogen-doped Reduced Graphene Oxide with Cobalt Tungstate Nanoparticles for Use in High-Performance Supercapacitors, *Appl. Surf. Sci*., 423(2017), 1025-1034.
55. M. Rahimi-nasrabadi, H. Reza, N. Meisam, S. Karimi, Cobalt carbonate and cobalt oxide nanoparticles synthesis, characterization and supercapacitive evaluation, *J. Mater. Sci. Mater. Electron*., 28(2017), 1877-1888.
56. H.R. Naderi, H.R. Mortaheb, A. Zolfaghari, Supercapacitive properties of nanostructured MnO_2/exfoliated graphite synthesized by ultrasonic vibration, *J. Electroanal. Chem*., 719(2014), 98-105.
57. J. Pu, Y. Tong, S. Wang, E. Sheng, Z. Wang, Nickel-cobalt hydroxide nanosheets arrays on Ni foam for pseudocapacitor applications, *J. Power Sources*, 250(2014), 250-256.
58. S. W. Chou, J. Y. Lin, Cathodic Deposition of Flaky Nickel Sulfide Nanostructure as an Electroactive Material for High-Performance Supercapacitors, *J. Electrochem. Soc*., 160(2013) D178-D182.
59. W. Hu, R. Chen, W. Xie, L. Zou, N. Qin, D. Bao, $CoNi_2S_4$ nanosheet arrays supported on Ni foams with ultrahigh capacitance for aqueous asymmetric supercapacitor applications, *ACS Appl. Mater. Inter.*, 6(2014), 19318-19326.

How to cite this article:
Z. Norouzi, S. H. Mahmoudi Najafi, S. A. Mozaffari, Facile One-pot Synthesis of Binder-free $MnCo_2O_4$ Nanosheets as Efficient Supercapacitor Electrode Material. Prog. Color Colorants Coat., 16 (2023), 271-281.